ARTICLES

Direct inhibition of the NOTCH transcription factor complex

Raymond E. Moellering[1,2,3], Melanie Cornejo[4], Tina N. Davis[6], Cristina Del Bianco[5], Jon C. Aster[5], Stephen C. Blacklow[5], Andrew L. Kung[6], D. Gary Gilliland[4,7], Gregory L. Verdine[1,3] & James E. Bradner[2,3,8]

Direct inhibition of transcription factor complexes remains a central challenge in the discipline of ligand discovery. In general, these proteins lack surface involutions suitable for high-affinity binding by small molecules. Here we report the design of synthetic, cell-permeable, stabilized α-helical peptides that target a critical protein–protein interface in the NOTCH transactivation complex. We demonstrate that direct, high-affinity binding of the hydrocarbon-stapled peptide SAHM1 prevents assembly of the active transcriptional complex. Inappropriate NOTCH activation is directly implicated in the pathogenesis of several disease states, including T-cell acute lymphoblastic leukaemia (T-ALL). The treatment of leukaemic cells with SAHM1 results in genome-wide suppression of NOTCH-activated genes. Direct antagonism of the NOTCH transcriptional program causes potent, NOTCH-specific anti-proliferative effects in cultured cells and in a mouse model of NOTCH1-driven T-ALL.

Transcription factors are master regulators of cell state. Commonly activated by genetic events or upstream signalling pathways, they mediate the neoplastic phenotype and maintain tissue specification in cancer. As such, they are highly desirable targets for ligand discovery[1]. Owing to expansive protein–protein interfaces and a general absence of hydrophobic pockets, transcription factors have proven among the most chemically intractable of all therapeutic targets. With the exception of nuclear hormone receptors that have evolved the ability to bind natural small-molecule ligands, potent and specific inhibitors of human transcription factors have not been realized. Here we report the successful development of a direct-acting antagonist of an oncogenic transcription factor, NOTCH1.

NOTCH proteins participate in conserved pathways that regulate cellular differentiation, proliferation and death[2,3]. Mammalian NOTCH receptors (NOTCH1–4 in humans) are single-pass transmembrane proteins that transmit juxtacrine signals initiated by ligands of the Delta, Serrate or Lag-2 family. Ligand binding to the extracellular domain of NOTCH1 initiates sequential proteolytic processing events catalysed respectively by an ADAM family metalloprotease and a γ-secretase complex, resulting in cytoplasmic release of the intracellular domain of NOTCH1 (ICN1)[4–6]. ICN1 then translocates to the nucleus and loads onto the DNA-bound transcription factor CSL[7]. The engagement of ICN1 with CSL creates a long, shallow groove along the interface of the two proteins that serves as a binding surface for co-activator proteins of the mastermind-like (MAML) family[8,9]. The resulting ICN–CSL–MAML ternary complex then recruits the core transcription machinery, effecting activation of NOTCH-dependent target genes.

The duration and strength of NOTCH signalling is normally tightly controlled. Whereas loss-of-function mutations have been observed in a variety of diseases[10–12], gain-of-function mutations in the NOTCH pathway are causally linked with cancer. Indeed, human *NOTCH1* was first discovered owing to its involvement in a t(7;9) chromosomal translocation observed in patients with T-ALL[13]. Subsequently, various activating mutations in *NOTCH1* have been discovered in >50% of patients with T-ALL[14]. Recently, further aberrations that potentiate NOTCH signalling have been identified, including loss-of-function of the NOTCH1 E3 ubiquitin ligase FBXW7 and the intracellular NOTCH inhibitor NUMB, in T-ALL and breast adenocarcinoma, respectively[15,16]. Activated NOTCH signalling has also been observed in cancers of the lungs, ovaries, pancreas and gastrointestinal tract as well as in melanoma, multiple myeloma and medulloblastoma[17–23].

Efforts to antagonize the NOTCH pathway have relied on blocking the generation of ICN using small-molecule inhibitors of the γ-secretase complex (GSIs)[24,25]. These molecules are not strictly NOTCH-specific, as they indiscriminately block the many signalling pathways downstream of γ-secretase[26]. T-ALL patients treated with GSIs suffer dose-limiting gastrointestinal toxicity, the origin of which is uncertain but it may result from chronic blockade of NOTCH1 and NOTCH2 processing[27]. Some cell lines containing activating *NOTCH1* mutations are resistant to GSIs, and those that do respond commonly undergo growth arrest rather than apoptosis. These observations underscore the mechanistic utility and potential therapeutic value of NOTCH antagonists that act by directly targeting the NOTCH transactivation complex.

Stapled α-helical peptides targeting the NOTCH complex

A dominant-negative fragment of MAML1 (residues 13–74; termed dnMAML1) has been shown to antagonize NOTCH signalling and cell proliferation when expressed in T-ALL cell lines[28,29]. In X-ray structures of the *Homo sapiens*[30] and *Caenorhabditis elegans*[31] core ICN–CSL–MAML complexes, this dnMAML1 polypeptide forms a nearly continuous α-helix that engages an elongated groove formed by the assembly of ICN1 and CSL (Fig. 1a). This α-helical interaction motif suggested that the NOTCH transactivation complex might be suitable for targeting by helix-mimetics such as hydrocarbon-stapled α-helical peptides, which in other systems have proven capable of targeting intracellular protein–protein interactions[32,33]. Specifically, we reasoned

[1]Department of Chemistry & Chemical Biology, Harvard University, Cambridge, Massachusetts 02138, USA. [2]Chemical Biology Program, Broad Institute of Harvard & MIT, Cambridge, Massachusetts 02142, USA. [3]Program in Cancer Chemical Biology, Dana-Farber Cancer Institute, Boston, Massachusetts 02115, USA. [4]Division of Hematology, Brigham & Women's Hospital, [5]Department of Pathology, Brigham & Women's Hospital, [6]Department of Pediatric Oncology, Dana-Farber Cancer Institute and Children's Hospital, [7]Howard Hughes Medical Institute, [8]Division of Hematologic Neoplasia, Dana-Farber Cancer Institute, Harvard Medical School, Boston, Massachusetts 02115, USA.

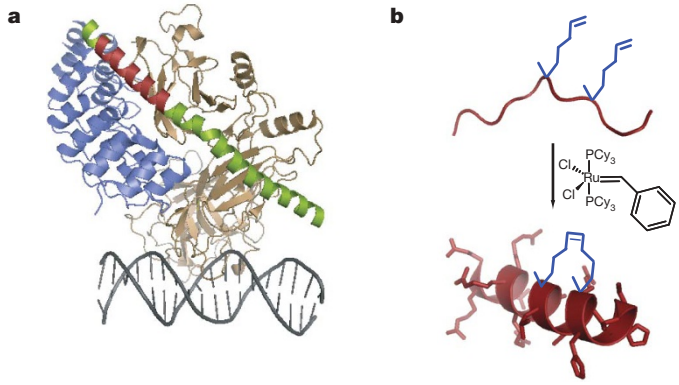

Compound	Sequence	Helicity
MAML1(21–36)	βAla-ERLRRRIELCRRHHST	23%
SAHM1–UN	βAla-ERLRRRI*LCR*HHST	40%
SAHM1	βAla-ERLRRRI*LCR*HHST	94%
SAHM2	βAla-SAVMERL*RRI*LCRRHH	73%
SAHM3	βAla-RIELCRRHH*TCE*RYEAV	59%
SAHM4	βAla-ERLELER*HTF*LHQR	67%
SAHM5	βAla-ELER*HTF*LHQR	72%
SAHM6	βAla-QHTFALH*RCI*AKAKR	56%
SAHM1–D1	βAla-RELRREI*LCR*HHST	83%
SAHM1–D2	βAla-RELRRRI*LCE*HHST	78%
dSAHM1	βAla-DRLRRRM*NYR*RQTD	55%

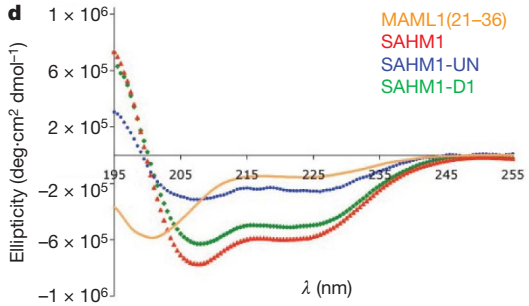

Figure 1 | Design of MAML1-derived stapled peptides targeting NOTCH1–CSL. a, Structure of the NOTCH1 ternary complex (Protein Data Bank (PDB) accession 2F8X): CSL (tan), DNA (grey), dnMAML1 (green) and ICN1 (blue). The 16-amino-acid stretch of MAML1 targeting ICN1 and CSL is shown in red, and was used to design the stapled peptide SAHM1. **b**, Schematic of peptide stapling. A non-natural alkenyl amino acid (S_5) is incorporated at two positions in the peptide chain and then cross-linked by ring-closing olefin metathesis. **c**, Schematic, sequences and helical character of MAML1-derived SAHM peptides. βAla denotes a β-alanine spacer. Asterisks denote the location of S_5 residues, which are cross-linked in all SAHM peptides except SAHM1-UN. **d**, Circular dichroism spectroscopy of four MAML1 derived peptides illustrating the incremental effects of synthetic modification.

that a stapled fragment of dnMAML1 might prevent binding of full-length MAML1 to the ICN1–CSL complex, thereby depriving the complex of its transcriptional activation function despite the presence of an upstream NOTCH signal. Relative to unmodified peptides, hydrocarbon-stapled peptides have shown improved binding affinity, metabolic stability and serum half-life. Operationally, peptide stapling is accomplished by co-synthetic incorporation of a non-natural amino acid, S_5, at neighbouring positions along one face of the α-helix (i and $i+4$ positions), followed by ring-closing olefin metathesis (Fig. 1b).

The structure of the human NOTCH1 ternary complex was used as the basis for the design of a series of stapled α-helical peptides derived from MAML1 (SAHMs). Six candidate peptides were designed that together scan the entire contact surface of dnMAML1 with ICN1–CSL (Fig. 1c). Functional evaluation of this panel led to the selection of a stapled peptide designated SAHM1, which spans residues Glu 21 to Thr 36. As shown in Fig. 1d and Supplementary Fig. 1, stapling conferred upon SAHM1 a marked increase in helical character, as compared with its unmodified and modified but unstapled counterparts (MAML1(21–36) and SAHM1-UN, respectively). As specificity controls for functional studies[34], we generated mutant peptides SAHM1-D1 and SAHM1-D2, as well as *d*SAHM1, the corresponding peptide from the *Drosophila* Mastermind (MAM) protein.

Analysis of cell penetration using fluorescein isothiocyanate (FITC)-labelled peptides and quantitative epifluorescence microscopy showed robust and roughly equivalent cellular uptake by FITC–SAHM1, FITC–SAHM2, FITC–SAHM3, FITC–SAHM6 and the negative control peptides FITC–SAHM-D1, FITC–SAHM-D2 and FITC–*d*SAHM1. Cell penetration was less efficient for FITC–SAHM4 and negligible for FITC–-SAHM5 (Supplementary Fig. 2a, b). The uptake of FITC–SAHM1 was diminished at 4 °C relative to 37 °C, and was unaffected by rhodamine conjugation, consistent with an active, endocytic peptide import mechanism as observed previously with stapled peptides (Supplementary Fig. 2c, d). The molecules in this study are considerably smaller than the ~25-kilodalton (kDa) exclusion size of the nuclear pore complex, and thus as expected, FITC–SAHM1 was distributed throughout the cytoplasm and nucleus (Supplementary Fig. 2e).

SAHMs bind the ICN1–CSL complex competitively with MAML1

SAHM binding to the NOTCH complex was first investigated using an *in vitro* pull-down assay. In brief, a glutathione-*S*-transferase (GST)-tagged fragment of ICN1 bearing only the CSL-binding domain (GST–RAMANK) was immobilized on glutathione-labelled agarose beads and used to precipitate CSL and dnMAML1 in the presence and absence of SAHM1 (Fig. 2a). SAHM1 inhibited dnMAML1 binding competitively, but did not perturb binding of CSL to RAMANK.

SAHM binding was next measured quantitatively using fluorescence polarization spectroscopy. Soluble FITC–SAHM1 was found to bind the pre-formed RAMANK–CSL complex with a dissociation constant (K_d) = 0.12 ± 0.02 μM, whereas the unmodified FITC–MAML1(21–36) peptide bound the complex with markedly diminished affinity (Fig. 2b). Thus, helix stabilization promotes target binding. The mutant peptides FITC–SAHM1-D1, FITC–SAHM1-D2 and FITC–*d*SAHM1 bound RAMANK–CSL considerably less avidly than FITC–SAHM1, prompting the use of these peptides as negative controls in subsequent functional studies. Notably, fluorescence polarization of FITC–SAHM1 was decreased by unlabelled competitor dnMAML1, confirming the overlap between the SAHM1 and the dnMAML binding sites on RAMANK–CSL (Fig. 2c).

Kinetic insights into complex assembly and SAHM binding were gained using surface plasmon resonance (SPR). A constant amount of GST–RAMANK was immobilized on an immunoglobulin (anti-GST) biosensor surface and exposed to increasing concentrations of CSL. The resulting dose-dependent response data were best fit to a two-step association with rapid on- and off-rates and overall micromolar affinity (Fig. 2d), and are consistent with a published model supporting a two-step association[34]. Next, SPR was used to analyse binding of SAHMs to the pre-assembled RAMANK–CSL complex. A SAHM1 derivative containing an amino-terminal biotin moiety (bioSAHM1) was immobilized on a streptavidin sensor surface. Pre-incubated, equimolar RAMANK and CSL were introduced in increasing concentrations. Curve-fitting of these kinetic data indicated that bioSAHM1 bound RAMANK–CSL with an apparent K_d closely matching the value observed by fluorescence polarization (Fig. 2e). Again, SAHM1-D1 showed substantially decreased affinity (Fig. 2f).

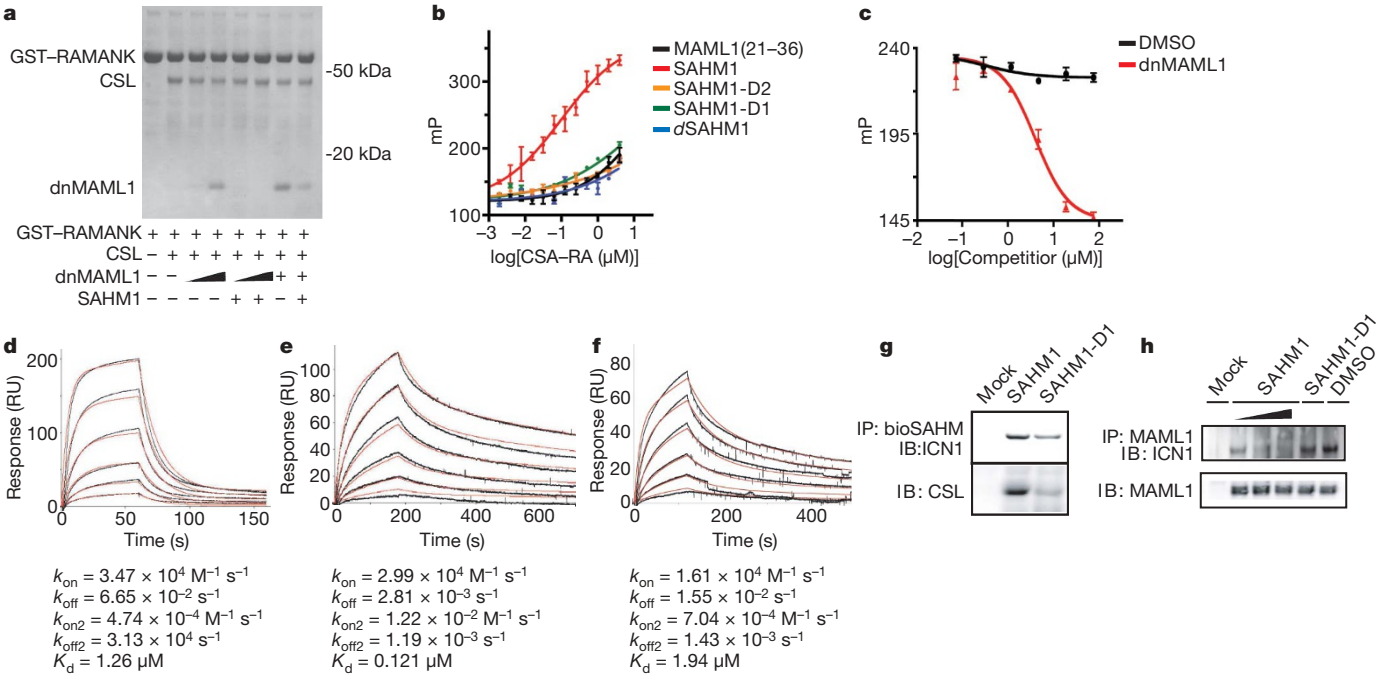

Figure 2 | SAHM1 specifically engages the NOTCH1 transactivation complex. a, *In vitro* assembly of the NOTCH1 complex. Bead-immobilized RAMANK protein was incubated as indicated with CSL (0.5 μM), dnMAML1 (0.5 μM for lanes 3 and 5 (from left); 2.5 μM for lanes 4 and 6; 5 μM for lanes 7 and 8), and SAHM1 (10 μM). Bound proteins were washed, eluted and resolved by gel electrophoresis (Coomassie). **b**, Fluorescence polarization of FITC–SAHM peptides binding to RAMANK–CSL. **c**, Direct competition between unlabelled dnMAML1 and FITC–SAHM1. Concentrations of FITC–SAHM1 (15 nM) and RAMANK–CSL (0.6 μM) were held constant. dnMAML1 IC_{50} = 3.9 ± 0.9 μM. **d**, CSL binding to immobilized RAMANK by SPR. Black curves represent sensogram data and the red curve denotes fit to a two-step kinetic model. Binding constants are shown. k_{on}, association rate; k_{off}, dissociation rate; RU, response units. **e**, **f**, Binding of RAMANK–CSL complexes to immobilized bioSAHM1 (**e**) and bioSAHM1-D1 (**f**). **g**, bioSAHM1 and bioSAHM1-D1 pull-down assays in KOPT-K1 lysates. Bound protein fractions were probed with antibodies specific for ICN1 (top) and CSL (bottom). **h**, Competitive co-immunoprecipitation of endogenous ICN1 by MAML1 in the presence of vehicle, SAHM1 (0.5, 1 and 10 μM from left to right) or SAHM1-D1 (10 μM). Unless noted otherwise data represent the mean ± s.d. (n = 3).

To determine whether SAHMs bind endogenous NOTCH proteins present in human T-ALL cells, we performed pull-down assays in KOPT-K1 cellular lysates. BioSAHM1 beads were found to pull down full-length ICN1 and CSL, whereas bioSAHM1-D1 was markedly less avid (Fig. 2g). Next we examined the ability of SAHMs to compete with endogenous MAML1, again in KOPT-K1 cellular lysates. After immunoprecipitation of MAML1, the presence of ICN1 was detected by immunoblot. This association was diminished in a dose-dependent manner by SAHM1 but not SAHM-1D (Fig. 2h). Together, these experiments demonstrate conclusively that SAHM1 binds ICN1 and CSL and thereby directly antagonizes recruitment of the MAML1 co-activator to the ICN1–CSL complex.

SAHM1 specifically represses NOTCH1 target gene expression

To explore the effects of SAHMs on transcriptional activity, we first used an established reporter-gene assay in which firefly luciferase is transcriptionally regulated by constitutively activated *NOTCH1* (ref. 35). SAHM1 treatment resulted in near complete repression of luciferase activity, comparable to a known GSI (DAPT)[25]. SAHM2 conferred a twofold signal reduction. SAHM4, SAHM5, SAHM6, SAHM1-D1, SAHM1-D2 and *d*SAHM1 were inactive (Fig. 3a). Reporter gene repression by SAHM1 was observed to be dose-dependent, with a half-maximum inhibitory concentration (IC_{50}) of 6.5 ± 1.6 μM (Fig. 3b). In a second reporter-gene assay monitoring β-lactamase transcriptionally regulated by ICN1 (ref. 36), SAHM1 again exhibited dose-dependent repression compared to SAHM1-D1 or vehicle alone (Supplementary Fig. 3a).

We next studied the effect of SAHMs on the expression of NOTCH target genes in NOTCH1-dependent T-ALL, quantified by PCR with reverse transcription (RT–PCR). A human T-ALL cell line (KOPT-K1) containing activating mutations in the heterodimerization (HD) and degradation domains (PEST) of *NOTCH1* was treated with SAHM1, SAHM1-D1 and vehicle. Decreased expression of the NOTCH1 target genes *HES1*, *MYC* and *DTX1* was uniquely observed after treatment with SAHM1 (Fig. 3c). A consistent repressive effect of SAHM1 on NOTCH1-dependent gene expression was observed across a panel of human T-ALL cell lines (Fig. 3d), containing diverse mutant *NOTCH1* alleles (Supplementary Table 1). SAHM1 had no effect on ICN1 protein stability compared to DAPT (Supplementary Fig. 3b), supporting transcriptional inhibition downstream of ICN1 production.

SAHM1 triggers global suppression of NOTCH1 signalling

Transcriptional profiling has recently been demonstrated to establish mechanistic connectivity between dissimilar compounds acting on common targets or target pathways[37]. Gene set enrichment analysis (GSEA) has also emerged as a robust method for comparing expression profiles corresponding to defined cellular states[38]. Integrating these two methodologies, we performed gene expression profiling as multidimensional phenotyping to first measure the global transcriptional effects of SAHM1 and then compare these effects with those produced by GSI treatment. First, triplicate data sets were generated from SAHM1 and vehicle-treated KOPT-K1 and HPB-ALL cells and analysed on Affymetrix oligonucleotide microarrays. Supervised hierarchical clustering and rank-ordering identified numerous canonical NOTCH1 target genes including *HES4*, *DTX1*, *HES1* and *MYC* among the top downregulated genes by SAHM1 (Fig. 3e). Next, a set of transcripts downregulated by GSI in T-ALL cell lines was curated from a published expression profile (referred to here as the GSI-NOTCH gene set)[39]. Enrichment for this gene set within the SAHM1 expression profile was studied by GSEA, revealing a strong, statistically significant correlation (enrichment score (ES) = −0.89,

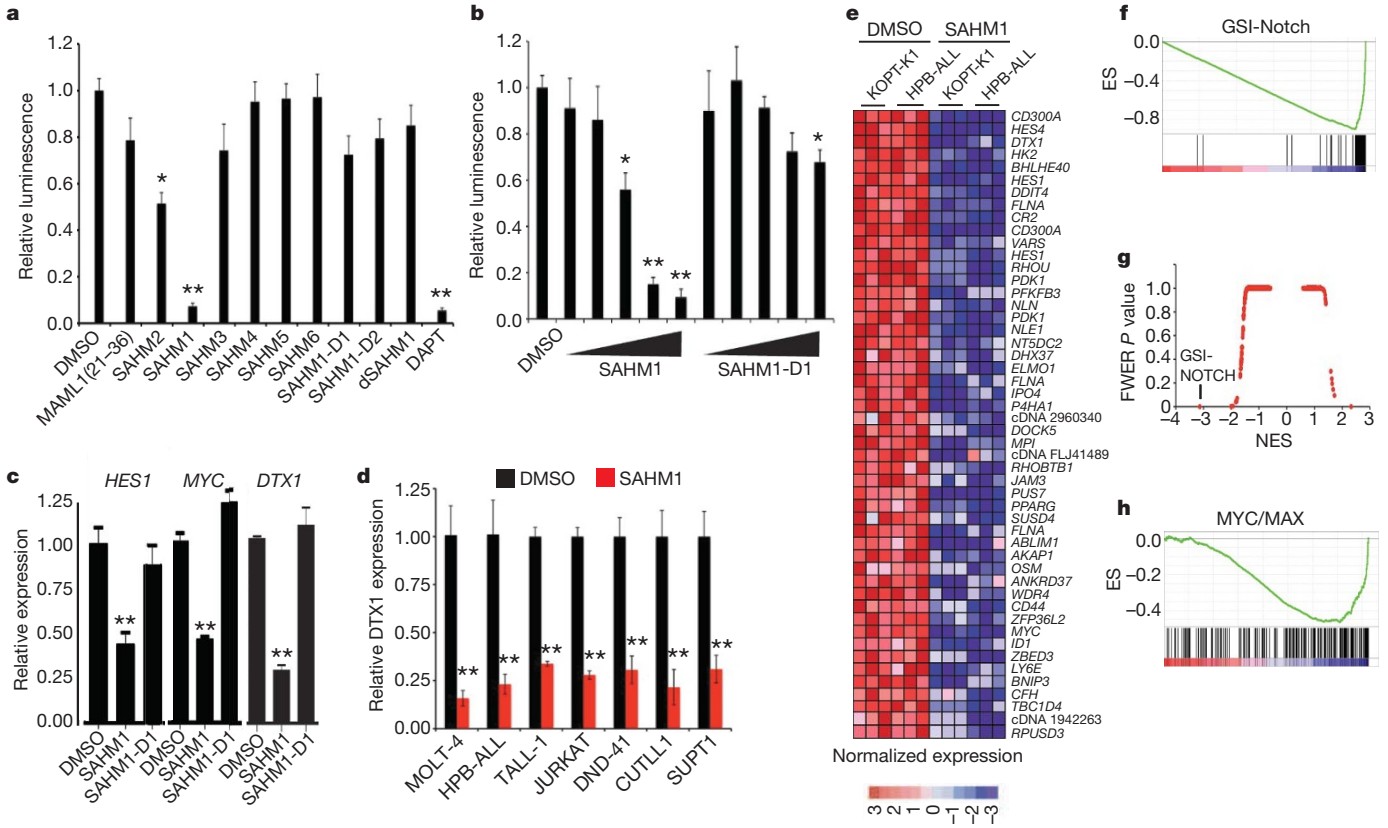

Figure 3 | SAHM1 represses NOTCH1 target gene expression. a, Inhibition of a NOTCH1-dependent luciferase reporter by SAHM peptides. Signal was normalized to *Renilla* luciferase control. **b**, Dose-dependent effects of SAHM1 and SAHM1-D1 in the dual-luciferase assay, using threefold dilutions (0.55–45 μM) of ligand compared to vehicle alone. **c**, qRT–PCR analysis of the *HES1*, *MYC* and *DTX1* mRNA levels in KOPT-K1 cells treated for 24 h with SAHM1 or SAHM1-D1 (20 μM) relative to dimethylsulphoxide (DMSO) control. **d**, qRT–PCR analysis of *DTX1* mRNA levels in a panel of human T-ALL cell lines. **e**, Heat map representation of the top 50 downregulated genes ($P < 0.001$), induced by SAHM1 in KOPT-K1 and HPB-ALL cells. **f**, Quantitative comparison of genes downregulated by GSI (GSI-NOTCH gene set) with the SAHM1 gene expression profile in KOPT-K1 and HPB-ALL cells by GSEA. **g**, Comparison of all transcription factor target gene sets in the Molecular Signatures Database to the GSI-NOTCH gene set for enrichment in the SAHM1 expression profile by GSEA. Data are plotted as the family-wise error rate (FWER) *P* value versus the NES. GSI-NOTCH is marked as the most enriched gene set. **h**, GSEA of the second most enriched gene set (MYC/MAX), applied to the SAHM1 expression profile. Unless noted otherwise data represent the mean ± s.d. ($n = 3$). $^*P < 0.05$, $^{**}P < 0.01$.

normalized ES (NES) = −3.66, $P < 0.0001$, Fig. 3f). Leading-edge analysis identified further enrichment for transcripts annotated as NOTCH1 targets in the scientific literature (Supplementary Fig. 4a). As a measure of biological specificity, enrichment analysis was conducted on all transcription factor target gene sets available in the Molecular Signatures Database (MSigDB). Taken together, the GSI-NOTCH gene set emerged as a statistical outlier as the most enriched in the SAHM1 profile (Fig. 3g and Supplementary Table 2). Interestingly, analysis of SAHM1-repressed genes also identified significant enrichment for gene sets regulated by transcriptional activators such as MYC/MAX and E2F, which have been previously identified as downstream targets of NOTCH activation (Fig. 3h and Supplementary Table 2)[40,41]. Taken together, these data establish that SAHM1 exerts a specific antagonistic effect on gene expression driven by NOTCH.

NOTCH inhibition halts the proliferation of T-ALL cells

Previous work has shown that chemical (GSIs) or genetic (dnMAML1 expression) inhibition of NOTCH induces cell-cycle arrest, apoptosis and decreased proliferative capacity in a subset of T-ALL cell lines[29,42]. We assembled a panel of genetically annotated T-ALL cell lines, which have previously demonstrated sensitivity to GSI (CUTLL1, SUPT1, HPB-ALL, TALL-1, DND-41 and KOPT-K1; Supplementary Table 1). SAHM1 treatment in these cells produced a marked reduction in cell proliferation whereas SAHM1-D1 was inactive (Fig. 4a). SAHM1 treatment did not affect the proliferation of K562 cells, an erythroleukaemia cell line without dependency on NOTCH1 for growth, or JURKAT and MOLT-4 cells, both of which are T-cell lines bearing activating NOTCH1 mutations but are insensitive to NOTCH inhibition owing to the loss of PTEN[15,41,43]. In sensitive T-ALL cell lines, SAHM1 exposure prompted activation of caspase 3 and 7, consistent with the induction of apoptosis (Fig. 4b).

These findings suggested that even brief exposure of T-ALL cells to SAHM1 might be sufficient to prevent the establishment of leukaemia *in vivo*. To recapitulate the human disease genotype and phenotype, we devised a murine model of T-ALL induced by the *NOTCH1* allele L1601PΔP, which bears dual NOTCH1 mutations originally identified in human T-ALL cells (Supplementary Fig. 5). Retroviral infection of the L1601PΔP allele into whole bone marrow followed by transplantation into lethally irradiated syngeneic recipient mice resulted in development of a T-ALL phenotype; primary cells demonstrated sensitivity to SAHM1 treatment *in vitro* (Supplementary Fig. 6a–c). To determine whether SAHM1 treatment could curb leukaemic engraftment, we pre-treated primary L1601PΔP cells with SAHM1 or vehicle before inoculation into secondary recipient mice (Supplementary Fig. 6d). At study end point, the SAHM1-treated cohort showed a statistically significant reduction in spleen weight (Fig. 4c) and the absolute number of donor-derived circulating lymphoblasts (Fig. 4d). Histopathological examination of bone marrow and spleen demonstrated a marked reduction in disease burden and leukaemic infiltration among animals administered SAHM1-treated cells (Fig. 4e).

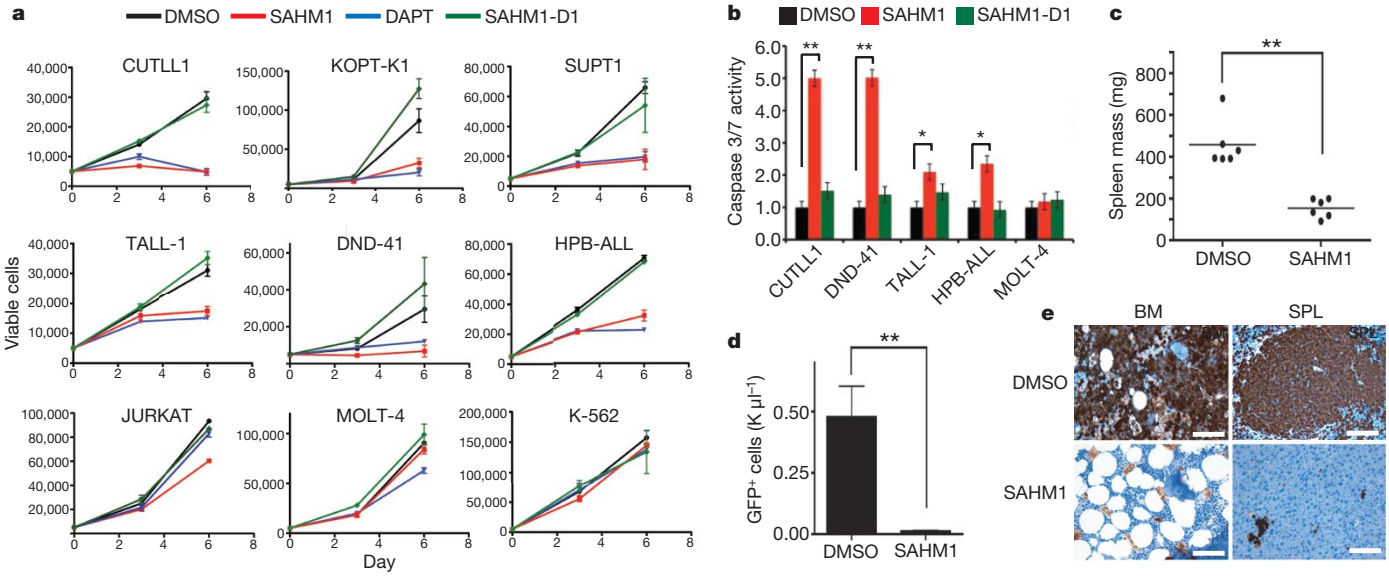

Figure 4 | SAHM1 reduces T-ALL proliferation and leukaemic initiation potential. **a**, Growth effects of SAHMs on a panel of human T-ALL cell lines of known mutational status. Cells were incubated with 15 µM DAPT (blue triangles), SAHM1 (red squares), SAHM1-D1 (green diamonds) or DMSO (black circles) and monitored for proliferation after 3 and 6 days of culture. Data points are mean ± s.d. ($n = 3$). **b**, Effects of SAHMs on apoptosis of T-ALL cells monitored using Capase-glo 3/7 (Promega) in cultures carried out as in **a**. Error bars, s.d. **c**, **d**, Ex-vivo treatment of L1601PΔP cells with SAHM1 (5 µM, 12 h) limits leukaemia initiation in secondary murine recipients. Reduction of spleen weight in the SAHM1 cohort ($n = 6$) compared to vehicle ($n = 6$) at the first sign of disease toxicity (23 days) ($P = 0.001$) (**c**). Circulating GFP-positive cell count in the blood is reduced by ~100-fold in the SAHM1 cohort ($n = 6$) relative to vehicle ($n = 6$) ($P = 0.0026$) (**d**). Error bars, s.d. Statistical analyses performed with a two-tailed *t*-test. $*P < 0.01$, $**P < 0.005$. **e**, An immunohistochemical stain for GFP that imparts a brown colour shows extensive leukaemic infiltration of bone marrow (BM) and spleen (SPL) in representative mice receiving vehicle-treated transplants relative to SAHM1. SPL, spleen. Scale bars,

SAHM1 inhibits leukaemic progression and NOTCH1 signalling

To evaluate whether SAHM1 treatment could attenuate the growth of established T-ALL *in vivo*, we developed a bioluminescent murine model of T-ALL. Either MIG-L1601PΔP or the control MIG retrovirus was used to infect bone marrow isolated from C57BL/6 mice in which firefly luciferase was constitutively expressed from the ubiquitin C promoter[44]. Infected cells were then transplanted into isogenic C57BL/6-Tyr$^{C/C}$ albino recipients to facilitate non-invasive bioluminescence imaging[45]. Animals transplanted with Luc-L1601PΔP cells developed progressive T-ALL (Fig. 5a) that was quantified by serial imaging (Fig. 5b), whereas no measurable disease developed in mice receiving control-transduced cells (Fig. 5a, b).

Balanced cohorts of secondary recipient mice with established leukaemia were treated with vehicle, daily SAHM1 (35 mg kg^{-1}), or twice-daily SAHM1 (30 mg kg^{-1}) by intraperitoneal injection. Vehicle-treated mice showed progressive disease, with eight out of nine mice showing increased bioluminescence over 5 days of treatment (Fig. 5c). Mice receiving daily SAHM1 treatments showed a slightly lower mean change in bioluminescence and included fewer animals with progressive disease (four out of six). All mice treated with twice-daily SAHM1, however, showed a significant dose-dependent regression of tumour as evidenced by a decrease in bioluminescence.

To confirm that the anti-leukaemic effect observed with SAHM1 treatment was associated with attenuated NOTCH1 signalling, mononuclear cells from vehicle- and SAHM1-treated (twice-daily) animals were collected for NOTCH1 target gene transcriptional analysis. A significant decrease in messenger RNA levels was evident for *Heyl*, *Hes1*, *Myc*, *Dtx1* and *Nrarp* in mice treated with SAHM1 compared to vehicle (Fig. 5d). Gene expression profiling also revealed significant pharmacodynamic repression of the NOTCH transcriptional program *in vivo*. A gene set of murine NOTCH1 targets was curated from a published report in which NOTCH1-dependent murine T6E cells were profiled after treatment with GSI or ectopic expression of dnMAML1 (ref. 40). Significant enrichment for the murine NOTCH1 gene set was observed in isolated cells from SAHM1-treated animals (Fig. 5e and Supplementary Fig. 7). Together, these data provide a direct link between inhibition of the NOTCH pathway and the anti-leukaemic activity of SAHM1 *in vivo*.

Discussion

Chemical intractability has limited the discovery of synthetic entities targeting transcription factors. Here we set out to assess whether a new type of targeting molecule, a stapled peptide derived from MAML1, could target a seemingly intractable transcription factor, human NOTCH1. We demonstrated direct binding to the pre-assembled form of the NOTCH1–CSL complex and competitive inhibition of MAML1 co-activator binding. Analysis of direct NOTCH1 target gene levels and the global expression profile induced by SAHM1 confirmed specific repression of the NOTCH signalling program in human and murine T-ALL cells. Given the complexities of transcriptional responses and the state of their characterization, it is impossible to rule out conclusively any off-target activity by SAHM1. In the context of human and murine T-ALL however, GSEA provides a striking correlation between the expression effects of SAHM1 and a GSI. Thus, it is clear that the NOTCH pathway is the major target of SAHM1. Direct transcriptional repression was subsequently found to enact NOTCH-specific anti-proliferative effects in annotated T-ALL cell lines. Finally, SAHM1 treatment curbed leukaemic progression and inhibited NOTCH1 signalling in a relevant murine model of T-ALL. Previous studies in mice and preliminary data in humans have shown that treatment with GSI alone is toxic owing to on-target effects on intestinal crypts, suggesting that different targeting strategies or drug combinations are needed; indeed recent reports are showing promise[46]. Our studies so far have not observed gastrointestinal toxicity at necropsy in treated animals (Supplementary Fig. 8a, b). Although expanded evaluation of SAHM1 as a possible therapeutic agent is needed, these early results indicate a potential therapeutic window.

As a direct transcriptional antagonist, SAHM1 should prove broadly useful in further determining the role of NOTCH in both normal tissues and disease processes, and presents a starting-point

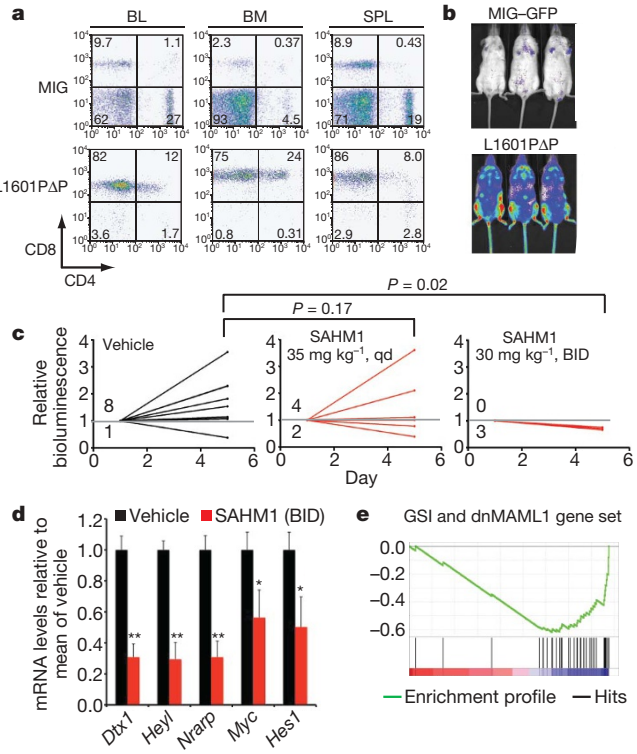

Figure 5 | SAHM1 treatment inhibits NOTCH signalling and leukaemic progression *in vivo*. **a**, Flow cytometric analysis of cells isolated from C57BL/6-Tyr$^{C/C}$ mice reconstituted with luciferase-expressing haematopoietic stem cells transduced with an L1601PΔP *NOTCH1* allele or empty vector (MIG). BL, blood. **b**, Bioluminescence imaging of primary recipients of Luc-L1601PΔP cells or control cells 2 months post-reconstitution. **c**, Bioluminescence quantification of tumour burden in mice with established disease treated with vehicle, 35 mg kg^{-1} SAHM1 per day (QD; $P = 0.17$), or 30 mg kg^{-1} SAHM1 twice daily (BID; $P = 0.02$). A Fisher's Exact test was used to compare disease progression between the cohorts. **d**, qRT–PCR analysis reveals repression of *Hes1* ($P = 0.0187$), *Myc* ($P = 0.023$), *Nrarp* ($P = 0.001$), *Heyl* ($P = 0.0006$) and *Dtx1* ($P = 0.0006$) mRNA levels in blood collected at day five from vehicle ($n = 3$) and SAHM1 (30 mg kg^{-1} BID, $n = 3$)-treated mice. **e**, Enrichment of GSI and dnMAML1 downregulated transcripts in the gene expression profile of leukocytes isolated from SAHM1-treated mice. Data in **d** represent the mean ± s.d. of triplicate measurements. Unless otherwise noted statistical analyses were performed with a two-tailed *t*-test. *$P < 0.05$, **$P < 0.005$.

for the development of a targeted therapeutic agent to treat NOTCH-driven cancers and non-malignant conditions. Furthermore, we expect the approach described here will prove broadly applicable to several other transcription factor complexes previously considered beyond the reach of ligand discovery.

METHODS SUMMARY

SAHM peptides were synthesized manually using standard 9-fluorenylmethoxycarbonyl (Fmoc)-peptide chemistry on MBHA rink amide resin, and cross-linked using Grubbs-I catalyst (benzylidene-bis(tricyclohexylphosphine)dichlororuthenium). Recombinant human CSL (amino acids 9–435), GST–RAMANK and RAMANK (amino acids 1761–2127 of NOTCH1) and dnMAML1 (amino acids 13–74) were expressed and purified as previously reported[47]. GST pull-down and fluorescence polarization experiments were performed in 20 mM Tris, pH 8.4, containing 150 mM NaCl, 1 mM EDTA and 1 mM dithiothreitol (DTT). SPR experiments were performed in the identical buffer with 187 mM NaCl and 0.01% P-20. Fluorescence polarization was measured at $\lambda_{ex} = 485$ nm and $\lambda_{em} = 525$ nm on a Perkin Elmer Spectramax-M5 multi-label plate reader. SPR experiments were performed on a Biacore S51 SPR instrument using anti-GST and streptavidin functionalized CM5 chips. Luciferase and β-lactamase reporter gene assays were performed as described[35,36]. For quantitative RT–PCR (qRT–PCR), RNA was extracted from T-ALL cells, reverse transcribed to complementary DNA, and amplified using standard primers and probes specific for human and murine transcripts. Expression values were calculated by the $2^{-\Delta\Delta C_t}$ method relative to the β-actin gene. RNA from triplicate SAHM- and vehicle-treated KOPT-K1 and HPB-ALL samples was used for analysis on Affymetrix U133 Plus 2.0 expression arrays, processed using GenePattern software. Gene set enrichment analysis was performed using GSEA software (http://www.broad.mit.edu/GSEA). Cell viability assays were performed in white, 96-well plates (Corning) in RPMI media containing 10% FCS. Fresh media and compounds were added every 3 days as needed. The L1601PΔP NOTCH1-dependent murine T-ALL cells were generated by reconstitution of lethally irradiated syngeneic mice with bone marrow cells transduced with the L1601PΔP NOTCH1 allele as described[48]. Luc-L1601PΔP animals were regularly monitored for bioluminescence, and euthanized at 2–3 months after transplant to obtain splenic T-ALL cells for secondary transplants and *in vivo* studies. Secondary recipients were monitored for leukaemia by bioluminescence and subsequently separated into treatment cohorts with matched disease burden.

Full Methods and any associated references are available in the online version of the paper at www.nature.com/nature.

Received 29 January 2009; accepted 25 September 2009.

1. Darnell, J. E. Jr. Transcription factors as targets for cancer therapy. *Nature Rev. Cancer* **2,** 740–749 (2002).
2. Artavanis-Tsakonas, S., Rand, M. D. & Lake, R. J. Notch signaling: cell fate control and signal integration in development. *Science* **284,** 770–776 (1999).
3. Bray, S. J. Notch signalling: a simple pathway becomes complex. *Nature Rev. Mol. Cell Biol.* **7,** 678–689 (2006).
4. Struhl, G. & Greenwald, I. Presenilin is required for activity and nuclear access of Notch in *Drosophila*. *Nature* **398,** 522–525 (1999).
5. Ye, Y., Lukinova, N. & Fortini, M. E. Neurogenic phenotypes and altered Notch processing in *Drosophila* Presenilin mutants. *Nature* **398,** 525–529 (1999).
6. De Strooper, B. *et al.* A presenilin-1-dependent γ-secretase-like protease mediates release of Notch intracellular domain. *Nature* **398,** 518–522 (1999).
7. Fortini, M. E. & Artavanis-Tsakonas, S. The suppressor of hairless protein participates in notch receptor signaling. *Cell* **79,** 273–282 (1994).
8. Petcherski, A. G. & Kimble, J. Mastermind is a putative activator for Notch. *Curr. Biol.* **10,** R471–R473 (2000).
9. Wu, L. *et al.* MAML1, a human homologue of *Drosophila* Mastermind, is a transcriptional co-activator for NOTCH receptors. *Nature Genet.* **26,** 484–489 (2000).
10. Li, L. *et al.* Alagille syndrome is caused by mutations in human *Jagged1*, which encodes a ligand for Notch1. *Nature Genet.* **16,** 243–251 (1997).
11. Joutel, A. *et al. Notch3* mutations in CADASIL, a hereditary adult-onset condition causing stroke and dementia. *Nature* **383,** 707–710 (1996).
12. Garg, V. *et al.* Mutations in *NOTCH1* cause aortic valve disease. *Nature* **437,** 270–274 (2005).
13. Ellisen, L. W. *et al. TAN*-1, the human homolog of the *Drosophila notch* gene, is broken by chromosomal translocations in T lymphoblastic neoplasms. *Cell* **66,** 649–661 (1991).
14. Weng, A. P. *et al.* Activating *mutations* of NOTCH1 in human T cell acute lymphoblastic leukemia. *Science* **306,** 269–271 (2004).
15. O'Neil, J. *et al. FBW7* mutations in leukemic cells mediate NOTCH pathway activation and resistance to γ-secretase inhibitors. *J. Exp. Med.* **204,** 1813–1824 (2007).
16. Pece, S. *et al.* Loss of negative regulation by Numb over Notch is relevant to human breast carcinogenesis. *J. Cell Biol.* **167,** 215–221 (2004).
17. Fre, S. *et al.* Notch signals control the fate of immature progenitor cells in the intestine. *Nature* **435,** 964–968 (2005).
18. Uyttendaele, H. *et al. Notch4/int-3*, a mammary proto-oncogene, is an endothelial cell-specific mammalian *Notch* gene. *Development* **122,** 2251–2259 (1996).
19. Nicolas, M. *et al.* Notch1 functions as a tumor suppressor in mouse skin. *Nature Genet.* **33,** 416–421 (2003).
20. Konishi, J. *et al.* γ-secretase inhibitor prevents Notch3 activation and reduces proliferation in human lung cancers. *Cancer Res.* **67,** 8051–8057 (2007).
21. Nefedova, Y., Cheng, P., Alsina, M., Dalton, W. S. & Gabrilovich, D. I. Involvement of Notch-1 signaling in bone marrow stroma-mediated de novo drug resistance of myeloma and other malignant lymphoid cell lines. *Blood* **103,** 3503–3510 (2004).
22. Park, J. T. *et al. Notch3* gene amplification in ovarian cancer. *Cancer Res.* **66,** 6312–6318 (2006).
23. Miyamoto, Y. *et al.* Notch mediates TGFα-induced changes in epithelial differentiation during pancreatic tumorigenesis. *Cancer Cell* **3,** 565–576 (2003).
24. Seiffert, D. *et al.* Presenilin-1 and -2 are molecular targets for γ-secretase inhibitors. *J. Biol. Chem.* **275,** 34086–34091 (2000).
25. Dovey, H. F. *et al.* Functional γ-secretase inhibitors reduce β-amyloid peptide levels in brain. *J. Neurochem.* **76,** 173–181 (2001).
26. Lleó, A. Activity of γ-secretase on substrates other than APP. *Curr. Top. Med. Chem.* **8,** 9–16 (2008).
27. Riccio, O. *et al.* Loss of intestinal crypt progenitor cells owing to inactivation of both Notch1 and Notch2 is accompanied by derepression of CDK inhibitors p27^{Kip1} and p57^{Kip2}. *EMBO Rep.* **9,** 377–383 (2008).
28. Maillard, I. *et al.* Mastermind critically regulates Notch-mediated lymphoid cell fate decisions. *Blood* **104,** 1696–1702 (2004).

29. Weng, A. P. *et al.* Growth suppression of pre-T acute lymphoblastic leukemia cells by inhibition of notch signaling. *Mol. Cell. Biol.* **23,** 655–664 (2003).
30. Nam, Y., Sliz, P., Song, L., Aster, J. C. & Blacklow, S. C. Structural basis for cooperativity in recruitment of MAML coactivators to Notch transcription complexes. *Cell* **124,** 973–983 (2006).
31. Wilson, J. J. & Kovall, R. A. Crystal structure of the CSL-Notch-Mastermind ternary complex bound to DNA. *Cell* **124,** 985–996 (2006).
32. Schafmeister, C. E., Po, J. & Verdine, G. L. An all-hydrocarbon cross-linking system for enhancing the helicity and metabolic stability of peptides. *J. Am. Chem. Soc.* **122,** 5891–5892 (2000).
33. Walensky, L. D. *et al.* Activation of apoptosis *in vivo* by a hydrocarbon-stapled BH3 helix. *Science* **305,** 1466–1470 (2004).
34. Del Bianco, C., Aster, J. C. & Blacklow, S. C. Mutational and energetic studies of Notch 1 transcription complexes. *J. Mol. Biol.* **376,** 131–140 (2008).
35. Aster, J. C. *et al.* Essential roles for ankyrin repeat and transactivation domains in induction of T-cell leukemia by notch1. *Mol. Cell. Biol.* **20,** 7505–7515 (2000).
36. Hallis, T. M. *et al.* An improved β-lactamase reporter assay: multiplexing with a cytotoxicity readout for enhanced accuracy of hit identification. *J. Biomol. Screen.* **12,** 635–644 (2007).
37. Lamb, J. *et al.* The Connectivity Map: using gene-expression signatures to connect small molecules, genes, and disease. *Science* **313,** 1929–1935 (2006).
38. Subramanian, A. *et al.* Gene set enrichment analysis: a knowledge-based approach for interpreting genome-wide expression profiles. *Proc. Natl Acad. Sci. USA* **102,** 15545–15550 (2005).
39. Palomero, T. *et al.* NOTCH1 directly regulates *c-MYC* and activates a feed-forward-loop transcriptional network promoting leukemic cell growth. *Proc. Natl Acad. Sci. USA* **103,** 18261–18266 (2006).
40. Weng, A. P. *et al.* c-Myc is an important direct target of Notch1 in T-cell acute lymphoblastic leukemia/lymphoma. *Genes Dev.* **20,** 2096–2109 (2006).
41. Rao, S. S. *et al.* Inhibition of NOTCH signaling by gamma secretase inhibitor engages the RB pathway and elicits cell cycle exit in T-cell acute lymphoblastic leukemia cells. *Cancer Res.* **69,** 3060–3068 (2009).
42. Lewis, H. D. *et al.* Apoptosis in T cell acute lymphoblastic leukemia cells after cell cycle arrest induced by pharmacological inhibition of notch signaling. *Chem. Biol.* **14,** 209–219 (2007).
43. Palomero, T. *et al.* Mutational loss of PTEN induces resistance to NOTCH1 inhibition in T-cell leukemia. *Nature Med.* **13,** 1203–1210 (2007).
44. Becker, C. M. *et al.* A novel noninvasive model of endometriosis for monitoring the efficacy of antiangiogenic therapy. *Am. J. Pathol.* **168,** 2074–2084 (2006).
45. Stubbs, M. C. *et al.* MLL-AF9 and FLT3 cooperation in acute myelogenous leukemia: development of a model for rapid therapeutic assessment. *Leukemia* **22,** 66–77 (2008).
46. Real, P. J. *et al.* γ-secretase inhibitors reverse glucocorticoid resistance in T cell acute lymphoblastic leukemia. *Nature Med.* **15,** 50–58 (2009).
47. Nam, Y., Weng, A. P., Aster, J. C. & Blacklow, S. C. Structural requirements for assembly of the CSL·intracellular Notch1·Mastermind-like 1 transcriptional activation complex. *J. Biol. Chem.* **278,** 21232–21239 (2003).
48. Chiang, M. Y. *et al.* Leukemia-associated *NOTCH1* alleles are weak tumor initiators but accelerate K-ras-initiated leukemia. *J. Clin. Invest.* **118,** 3181–3194 (2008).

Supplementary Information is linked to the online version of the paper at www.nature.com/nature.

Acknowledgements We thank S. Schreiber and the Broad Institute Chemical Biology Program for discussions and access to instrumentation; J. Rocnik for assistance in the establishment of the T-ALL murine model; A. Ferrando for providing GSI microarray data; M. Hancock and Invitrogen for providing β-lactamase HeLa reporter clones; K. Ross and A. Subramanian for conversations and guidance about GSEA; and S. Gupta and the Broad Institute Microarray Core. This work was supported by a Specialized Center of Research grant from the Leukaemia & Lymphoma Society (to J.E.B., J.C.A., S.C.B.), an AACR Centennial Pre-doctoral Research Fellowship in Cancer Research (to R.E.M.), the American Society of Hematology (to J.E.B.), MCCB-NIH Training Grant No. 5T32GM007598 (to R.E.M.), the Human Frontier Science Program (to C.D.), and the Harvard & Dana Farber Program in Cancer Chemical Biology (to J.E.B., R.E.M., G.L.V.). The project has been funded in part with Federal funds from the National Cancer Institute's Initiative for Chemical Genetics, National Institutes of Health, under Contract No. N01-CO-12400. Histology and immunohistochemical staining was performed in the Dana Farber/Harvard Cancer Center Specialized Histopathology Services Core Laboratory.

Author Contributions R.E.M., G.L.V. and J.E.B. conceptualized the study, designed the experiments, interpreted data, and wrote the manuscript. Design, synthesis and biological characterization of SAHM peptides was performed by R.E.M. C.D.B., J.C.A. and S.C.B. contributed key reagents and analysed data. R.E.M., M.C., T.N.D., J.C.A., A.L.K., D.G.G. and J.E.B. established the bioluminescent T-ALL model, designed and performed *in vivo* experiments and analysed data.

Author Information All microarray data has been deposited to the Gene Expression Omnibus at the National Center for Biotechnology Information under accession numbers GSE18198 and GSE18351. Reprints and permissions information is available at www.nature.com/reprints. The authors declare competing financial interests: details accompany the full-text HTML version of the paper at www.nature.com/nature. Correspondence and requests for materials should be addressed to J.E.B. (james_bradner@dfci.harvard.edu) or G.L.V. (gregory_verdine@harvard.edu).

METHODS

Chemical reagents. Solid phase rink amide MBHA resin (100–200 mesh), 2-(6-chloro-1H-benzotriazole-1-yl)-1,1,3,3-tetramethylaminium hexafluorophosphate (HCTU), natural Fmoc-protected L-amino acids and *N*-biotinyl-NH-PEG_2-COOH were all purchased from Novabiochem (EMD Chemicals). The γ-secretase inhibitor *N*-[*N*-(3,5-difluorophenacetyl-L-alanyl)]-*S*-phenylglycine *t*-butyl ester (DAPT) was purchased as a 25 mM solution in DMSO from Calbiochem (EMD Chemicals). All other reagents and solvents for chemical synthesis were purchased from Sigma Aldrich.

Solid-phase peptide synthesis. All peptides were synthesized manually using standard Fmoc-peptide chemistry on MBHA rink amide resin. Chemical cross-linking of non-natural amino acids containing pentenyl side-chains was performed using 0.1 equivalents of Grubbs-I catalyst (benzylidene-bis(tricyclohexylphosphine)dichlororuthenium) dissolved in dichloroethane under Argon for 2.5 h. After olefin-metathesis, peptides were subjected to one final round of deprotection and capping by standard methods with acetic anhydride, FITC or *N*-biotinyl-NH-PEG_2-COOH creating SAHM, FITC–SAHM and bioSAHM peptides, respectively. After completion, crude peptide was then dissolved in 1:1 acetonitrile:water, and purified by reverse-phase high-pressure liquid chromatography (HPLC) using a C18 column (Agilent). Compound identification and purity was assessed using coupled liquid chromatography mass spectrometry (LCMS) (Agilent).

Synthesis of non-natural amino acids was performed as reported[49].

Determination of α-helicity. A circular dichroism spectrometer (Jasco J-710) was used to determine the α-helical content of all SAHM peptides. SAHMs were dissolved into deionized water at pH 7.4 to a final concentration of 25–100 μM in a quartz cuvette with a path length of 1 cm. Absorbance values were taken at 1 nm intervals between 190 and 255 nm. The percentage helicity was calculated from the absorbance at 222 nm using helical models as previously reported in ref. 50.

Protein expression and purification. Human CSL (residues 9–435) was expressed with a carboxy-terminal hexahistidine tag in *Escherichia coli* strain BL21(DE3) pLysS (Stratagene) using a pET28a vector (Novagen). Transformed bacteria was grown at 18 °C and induced with 0.5 mM isopropyl-β-D-thiogalactoside (IPTG) at an $A_{600} = 0.8$. Cells were pelleted 14 h after induction and lysed in buffer 1 (50 mM Tris, pH 8.4, 500 mM NaCl, 2 mM DTT, 1 mM EDTA and 1 mM phenylmethylsulphonyl fluoride (PMSF)) by sonication. The lysate was centrifuged to clear insoluble matter before loading onto Ni-NTA resin (Qiagen). Column-bound protein was eluted using 250 mM imidazole in buffer 1 and concentrated by centrifugation using a 30-kDa exclusion filter. The concentrated eluent was dialysed into buffer 2 (20 mM Tris, pH 8.4, 1 mM DTT, 1 mM EDTA and 150 mM NaCl) before further purification by gel filtration on a Superdex-75 Column (Amersham Pharmacia Biotech). Human RAMANK (amino acids 1761–2127) of ICN1 was expressed and purified as reported[47]. The corresponding GST-fusion protein was bound to glutathione-Sepharose beads, which were washed with buffer 1 without protease inhibitors. The protein was then eluted from the beads with a solution of 20 mM gluthatione in buffer 1 to obtain GST–RAMANK, or cleaved directly from the resin using TEV protease to obtain RAMANK. Both proteins were further purified by gel filtration.

GST pull-down assays. Glutathione-functionalized agarose beads (GST-Bind, Biorad) were incubated with saturating concentrations of purified GST–RAMANK in buffer 2 for 30 min at 4 °C. Beads were washed and 40 μl of the 50% bead slurry was incubated with indicated mixtures of purified CSL (0 or 0.5 μM), dnMAML1 (0, 0.5, 2.5 or 5 μM) and SAHM1 (0 or 10 μM) to a final volume of 350 μl, and incubated for 1 h at 4 °C. Beads were washed four times with buffer 2, taken up in SDS–PAGE loading buffer, boiled, and SDS–PAGE was performed to visualize bound proteins by Coomassie staining.

Fluorescence polarization assays. SAHM-binding assays were performed by incubating FITC–SAHM peptides (15 nM) with twofold dilutions of equimolar RAMANK and CSL protein in buffer 2. Dilutions and incubations were made in 384-well, black flat-bottom plates (Corning) to a total volume of 40 μl, and equilibrated for 30 min. Polarization was measured on a Spectramax-M5 multi-label plate reader with $\lambda_{ex} = 485$ nm and $\lambda_{em} = 525$ nm. Polarization was calculated according to the standard equation: $P = (V - H)/(V + H)$, in which P denotes polarization, V denotes vertical emission intensity, and H represents horizontal emission intensity. K_d values were determined by fitting data to a variable-slope sigmoidal binding curve using Prism 4 graphing software. Competitive fluorescence polarization assays were performed by incubating fourfold dilutions of dnMAML1 or DMSO alone with FITC–SAHM1 (15 nM) and a pre-equilibrated mixture of RAMANK–CSL complex (600 nM). Polarization measurements and calculations were performed as above for binding assays.

Surface plasmon resonance. A Biacore S51 SPR-Instrument (Biacore-GE) was used for all SPR-binding measurements. Binding between the RAMANK domains of ICN1 and CSL was performed by first immobilizing IgG anti-GST (Pierce) on a CM5 Biacore chip by amine coupling with EDC (1-ethyl-3-[3-dimethylaminopropyl]carbodiimide hydrochloride) activation and NHS (*N*-hydroxysuccinimide) coupling. All proteins were exchanged into binding buffer (187 mM NaCl, 20 mM Tris, pH 8.4, 1 mM DTT and 0.05% P-20) before use. GST–RAMANK (50 μg ml^{-1}) was injected at a rate of 10 μl min^{-1} for 10 min, immobilizing approximately 400 response units. Escalating concentrations of CSL (twofold dilutions between 4.0 and 0.125 μM, including two blanks) were subsequently passed over the GST–RAMANK functionalized chip as well as an anti-GST reference surface. After each CSL dilution the sensor surface was regenerated with pH 2.2 Tris-glycine solution and again functionalized with a comparable level of GST–RAMANK to avoid carry-over between experiments. Binding data was reference normalized and processed using ClampXP software (http://www.cores.utah.edu/interaction/clamp.html). A two-site binding model was applied to the processed data set to determine kinetic parameters of the RAMANK–CSL interaction. SAHM binding to the RAMANK–CSL complex was performed using SAHM1 and SAHM1-D1 each capped at the N terminus with *N*-biotinyl-NH-$(PEG)_2$-COOH (Novabiochem). Peptides were dissolved in binding buffer and injected at 10 μl min^{-1} for 10 min into a flow cell containing a Streptavidin-CM5 Biacore chip. Equimolar dilutions of RAMANK and CSL (twofold dilutions from 1 to 0.03125 μM, including two blanks) were mixed in binding buffer and injected onto the peptide-functionalized surface to measure their association and dissociation to SAHM1 and SAHM1-D1. As with the RAMANK–CSL interaction, kinetic and thermodynamic data was generated using a two-site binding model in ClampXP software.

Western blots and co-immunoprecipitation assays. For ligand pull-down assays, biotinylated SAHMs were immobilized on Streptavidin-agarose beads (30 μl slurry) in 250 μl lysis buffer for 4 h at 4 °C. Separately, 2×10^6 KOPT-K1 cells were lysed in 20 mM Tris, pH 8, 150 mM NaCl, 1% Triton X-100, 0.1 mM NaF, 1 mM PMSF, 1 mM sodium orthovanadate and 2.5 μg ml^{-1} leuptin supplemented with complete-mini protease inhibitor (Roche) by sonication, followed by removal of insoluble debris by centrifugation at 4 °C. Clarified lysates were added to the SAHM-immobilized beads and incubated overnight. Beads were washed repeatedly with lysis buffer before the elution of bound proteins by boiling in gel-loading buffer for 10 min. Eluted proteins were processed for western blotting by standard methods using polyclonal antibodies specific for ICN1 (Val1744, Cell Signaling) or CSL (CBF-1, Santa Cruz Bio.). MAML1 immunoprecipitations were performed and analysed in a similar manner. Antibodies directed at MAML1 (Cell Signaling Technologies) were immobilized on Protein-A agarose beads for 4 h and washed with lysis buffer. Separately, cellular lysates were incubated with soluble FITC–SAHM in a total volume of 250 μl for 4 h at 4 °C. Lysates were then added to antibody-bound beads, incubated overnight and processed for western blot analysis as described earlier.

Fluorescence microscopy. High content imaging measurements were made using an IXMicro epifluorescence microscope (Molecular Devices Corporation) and quantified using MetaXpress image analysis software. To determine intracellular penetration, 2×10^3 cells were seeded in black, clear-bottom 384-well imaging plates (Costar) and incubated in 40 μl RPMI (KOPT-K1 cells) or DMEM (U2OS cells) media supplemented with 10% FBS and the compounds of interest. SAHM peptides (5 μM) were incubated with U2OS cells for 12 h at 37 °C. Cells were then washed three times with PBS, fixed with 3.7% formaldehyde in PBS, and counterstained with Hoescht dye (1:5,000). Epifluorescent images were taken in triplicate, imported into MetaXpress software, and scored as positive or negative on the basis of minimum size, maximum size, fluorescence intensity above local background and overlap of Hoescht and FITC signals. Rhodamine-labelled SAHM1 was visualized and scored in the same manner. The temperature dependence of SAHM1 penetration was determined in U2OS cells incubated with 5 μM FITC–SAHM1 for 4 h at either 37 °C or 4 °C as earlier.

Luciferase reporter gene assays. CSL-dependent luciferase reporter assays were performed as reported[35].

β-lactamase reporter gene assays. HeLa cells containing an integrated CSL-responsive β-lactamase transgene and a doxycycline-inducible ICN1 transgene were generously provided by Invitrogen. Cells were maintained under selection in DMEM containing 10% FBS, 5 μg ml^{-1} blasticidin, 125 μg ml^{-1} hyrgromycin and 75 μg ml^{-1} zeocin. Cells were seeded in 384-well imaging plates and ICN1 was induced with 150 ng ml^{-1} doxycycline for 24 h. After induction, stock solutions of SAHM peptides, potassium clavulanate or DMSO were added and cells were incubated for a further 24 h. The β-lactam fluorescence resonance energy transfer (FRET) substrate loading solution was prepared separately according to the manufacturer's specifications (ToxBlaZer substrate, Invitrogen Corp.). FRET loading solution (5 μl) was added to each induced well, and also to non-induced and cell-free wells to determine basal FRET ratio levels and fluorescence background, respectively. After 2 h, fluorescence measurements were made using

a Spectramax-M5 multi-label plate reader (Molecular Devices). The FRET probe was excited at 409 nm, and the emission values at 460 nm (cleaved probe) and 530 nm (intact probe) were measured. The background fluorescence of cell-free wells at both wavelengths was subtracted before calculating the 460 nm/530 nm emission ratio.

Quantitative RT–PCR. One-million human T-ALL cells were seeded in 24-well plates in RPMI containing 10% FCS. SAHM peptides (20 μM) were added and cells were then incubated for 24 h at 37 °C. RNA samples were prepared using an RNEasy Mini kit (Qiagen). Total RNA was reverse transcribed to cDNA using SuperScript II Reverse Transcriptase Kit according to the manufacturer's protocol (Invitrogen). The resulting cDNA was used as the substrate to measure relative expression levels by qRT–PCR with TaqMan (Applied Biosystems) probes and primers specific for human *HES1*, *MYC*, *DTX1* and *ACTB* for normalization: probe IDs Hs00172878_m1, Hs00153408_m1, Hs01092201_m1 and Hs99999903_m1, respectively. In other experiment involving murine T-ALL cells, the following TaqMan probes and primers specific for murine *Hes1*, *Myc*, *Dtx1*, *Nrarp*, *Heyl* and *Actb* were used: Mm01342805_m1, Mm00487807_m1, Mm00492297_m1, Mm00482529_s1, Mm00516555_m1 and Mm01205647_m1, respectively. Triplicate reactions were prepared in 384-well optical PCR plates (Applied Biosystems) and qPCR was performed using a ABI Prism 7900 (Applied Biosystems) instrument with the following run specifications: FAM probe detection, AmpErase activation for 2 min at 50 °C, DNA polymerase activation for 10 min at 95 °C, followed by 40 cycles of duplex melting for 15 s at 95 °C and annealing for 1 min at 60 °C. Threshold-cycle (C_t) values were automatically calculated for each replicate and used to determine the relative expression of the gene of interest relative to reference genes for both treated and untreated samples by the $2^{-\Delta\Delta Ct}$ method.

Gene expression profiling. One-to-two micrograms of RNA per array was prepared from cultures of KOPT-K1 and HPB-ALL cells treated for 24 h with 20 μM SAHM1 or equivalent DMSO as described earlier for qRT–PCR in triplicate. Expression profiles were then generated by hybridizing processed RNA with Human Genome U133 Plus 2.0 arrays (Affymetrix). Murine T-ALL gene expression profiles were generated with RNA isolated from vehicle and SAHM1-treated mice using Affymetrix Mouse 430 2.0 arrays. cDNA processing, chip preparation, hybridization and chip scanning were performed by the Broad Institute Microarray Core Facility. Raw .cel files were processed and normalized by the robust multiarray averaging (RMA) method using GenePattern software (http://www.broad.mit.edu/cancer/software/genepattern/). For the KOPT-K1 and HPB-ALL samples, RMA processed data was subsequently normalized to the mean of DMSO-treated samples on a per gene basis to control for interarray differences. The GSI-NOTCH gene set was compiled from the published GSI study by extracting the top gene identifiers consistently downregulated across seven T-ALL cell lines by signal-to-noise ratio. This list of probes was applied to the SAHM1 expression profile by GSEA software (http://www.broad.mit.edu/GSEA/). For the global analysis of all transciption factor target gene sets (C3 TFT gene sets) we downloaded a .gmt file containing all gene sets and added in the curated GSI-NOTCH gene set. This resulting .gmt database was queried against the SAHM1 expression profile with the following parameters: probe set collapse = true; phenotype = SAHM1 versus DMSO; permutation: gene set, permutations = 1,000. Gene set size: $15 < n < 500$. The MYC/MAX gene set in Fig. 3h is the second most enriched gene set titled 'V$MYCMAX_01' in the MSigDB.

Cell proliferation and apoptosis assays. Five-thousand cells were seeded in white, 96-well plates (Corning) in a total volume of 125 μl RPMI media containing 1% penicillin/streptomycin and 10% FBS. Media also contained 15 μM DAPT, SAHM1, SAHM1-D1 or equivalent concentrations of DMSO (0.3%). Cells were incubated at 37 °C for 72 h; at this point, the media was changed and fresh compounds added. The viable cell number was determined at 72 h and 144 h using the Cell Titer-Glo viability assay (Promega). All measurements were made in triplicate, and the growth curves shown are representative of several independent experiments. Apoptosis was determined at 144 h using the Caspase-Glo 3/7 assay (Promega), which reports on the activation of caspases 3 and 7 using a pro-luminescent substrate.

Viral infection and bone marrow transplantation. The MSCV-L1601P-ΔPEST-GFP (L1601PΔP) construct and the preparation of viral supernatants have been described[48]. Transduction efficiency in primary cells was confirmed by flow cytometric analysis of GFP expression. For bone marrow transplantation, 8–10-week-old wild-type Balb/c donor mice or $Tyr^{-/-}$, C57BL/6, Ubc-Luc mice were injected with 5-FU (Sigma) 6 days before bone marrow collection from femurs and tibiae. After an overnight incubation in RPMI-1640 supplemented with 10% FBS, 10 ng ml^{-1} mouse IL-3, 20 ng ml^{-1} mouse IL-6 and 10 ng ml^{-1} mouse SCF, cells were spin-infected with viral supernatants twice over 2 days. Transduced cells (1×10^6) were injected into the tail-vein of lethally irradiated syngeneic recipient mice. Animals were euthanized 2–3 months after transplant to obtain splenic T-ALL cells for secondary transplants and *in vivo* studies.

Leukaemia initiation studies. Primary murine T-ALL cells expressing L1601PΔP were re-suspended in 10% FBS-supplemented RPMI at a density of 1×10^6 cells per ml in 6-well plates. SAHM peptides or DMSO vehicle were added to a final concentration of 5 μM in 6 ml of media, and incubated with the cells for 12 h at 37 °C. Cells were then pelleted, resuspended in 3 ml of HBSS, and injected by tail vein (1×10^6 cells per mouse) into two cohorts of syngeneic Balb/c mice ($n = 6$) that had been sub-lethally irradiated 12 h previously. The primary end point of this *in vivo* study was spleen weight; secondary end points include peripheral blood counts and GFP$^+$ blood counts just before necropsy. Approval for animal use in this study was granted by the Children's Hospital Boston Animal Care and Use Committee.

***In vivo* efficacy experiments.** Primary and secondary recipients were generated as above using Ubc-Luc C57BL/6-$Tyr^{C/C}$ mice. Secondary recipients were monitored for leukaemic engraftment and progression using bioluminescent imaging as previously described[45]. Approximately 2–3 weeks after reconstitution, mice showing established disease were divided into cohorts for treatment with vehicle alone (5% DMSO in HBS), 35 mg kg^{-1} SAHM1 once per day, or 30 mg kg^{-1} SAHM1 twice per day, given intraperitoneally. At the end of 5 days of treatment, mice were again imaged to determine leukaemic progression, and euthanized to examine the pharmacodynamic effects of the various treatments on NOTCH1 target-gene expression. Blood was collected by terminal cardiac bleed from mice treated with vehicle ($n = 3$) or SAHM1 (30 mg kg^{-1} twice daily, $n = 3$) for qPCR and microarray gene expression analysis.

Histopathological analysis and immunohistochemistry. Paraffin-embedded tissue sections were prepared at the Dana Farber/Harvard Cancer Center Specialized Histopathology Services Core or Rodent Histopathology Core. In brief, tissues were fixed for at least 72 h in 10% neutral-buffered formalin (Sigma), dehydrated in alcohol, cleared in xylene, and infiltrated with paraffin on an automated processor (Leica). Tissue sections (4-μm thick) were placed on charged slides, deparaffinized in xylene, rehydrated through graded alcohol solutions, and stained with haematoxylin and eosin (H&E) or with anti-CD3 (Cell Marque), anti-B220 (BD Pharmingen), or anti-Ki-67 (Dako) antibodies. Images were obtained using an Olympus BX40 microscope (Olympus Imaging America) and a Micropublisher 3.3 RTV colour camera (QImaging).

Flow cytometry. All antibodies were obtained from BD Pharmingen and staining procedures were performed in PBS, 2% FBS. Freshly collected splenocytes or bone marrow cells (0.5×10^6 per condition) were blocked with anti-CD16/32 antibody for 10 min and then incubated with 2 μl of each specific antibody for 30 min on ice in the dark. After two washes with PBS, 2% FBS, cells were resuspended in 200 μl PBS and analysed by flow cytometry. All analyses were gated on GFP$^+$ cells.

49. Williams, R. M. & Im, M. N. Asymmetric synthesis of monosubstituted and α, α-disubstituted α-amino acids via diastereoselective glycine enolate alkylations. *J. Am. Chem. Soc.* **113**, 9276–9286 (1991).
50. Chen, Y. H., Yang, J. T. & Chau, K. H. Determination of the helix and β form of proteins in aqueous solution by circular dichroism. *Biochemistry* **13**, 3350–3359 (1974).

ERRATUM

doi:10.1038/nature08660

Direct inhibition of the NOTCH transcription factor complex

Raymond E. Moellering, Melanie Cornejo, Tina N. Davis, Cristina Del Bianco, Jon C. Aster, Stephen C. Blacklow, Andrew L. Kung, D. Gary Gilliland, Gregory L. Verdine & James E. Bradner

Nature 462, 182–188 (2009)

In the print issue of this Article, text from the last line of the Figure 4 legend, defining the scale bar lengths, is inadvertently missing. This sentence should read ''Scale bars, 50 μm''.